Modeling and Dosimetry of Monoclonal Antibody M195 (Anti-CD33) in Acute Myelogenous Leukemia

George Sgouros, Martin C. Graham, Chaitanya R. Divgi, Steven M. Larson and David A. Scheinberg

Medical Physics, Nuclear Medicine Service and Leukemia Service, Memorial Sloan-Kettering Cancer Center, New York, New York

Individual patient response to radioimmunotherapy is influenced by each patient's tumor burden, antibody clearance kinetics and the antibody-antigen interaction. In hematologic malignancies, wherein antibody access to tumor-cell associated antigen is rapid, mathematical modeling may provide a quantitative basis for assessing the impact of patient variability on a particular therapeutic protocol. Compartmental modeling analysis of antibody pharmacokinetics from a Phase I trial of ^{131}I-labeled monoclonal antibody, M195 (anti-CD33), was used to estimate tumor burden in cases of acute myelogenous leukemia and the absorbed dose in liver, spleen and red marrow. The suitability of a nonlinear, two-compartment model for simulating M195 distribution in leukemia patients was evaluated by comparing model predictions with patient measurements. The results demonstrate that for directly accessible, hematologically distributed tumor cells, a two-compartment model fits observed patient biodistribution data and may provide information regarding both total tumor burden and tumor burden in the liver, spleen and red marrow. The model also provides biodistribution information for absorbed dose calculations to tissues that are not directly sampled. Such information is important in determining the optimum therapeutic dose of radiolabeled antibody for a given patient.

J Nucl Med 1993; 34:422–430

The use of radiolabeled antibodies for cancer therapy requires specification of two basic parameters: the amount of antibody that should be administered and the amount of radioactivity that should accompany the antibody. A systematic approach to the selection of these two parameters must include consideration of each patient's tumor burden, antibody clearance kinetics and the antibody-antigen interaction.

Previous models of the gross distribution of radiolabeled antibodies have yielded important general guidelines regarding plasma and organ kinetics as a function of antibody dose (*1,2*). The work of Eger et al. (*3*) and Covell et al. (*4*) demonstrated that fits to these tissues could be obtained by apportioning the contents of several compartments to each of these organs due to the sinusoidal nature of liver, spleen and marrow vasculature. Sung et al. (*5*) have compared animal biodistribution data for antibody-antigen combinations exhibiting different binding parameters with a mathematical model to demonstrate the relative importance of binding affinity and tumor cell antigen density on antibody uptake. Zanzonico et al. (*6*) used the results of a compartmental model fit to patient data to generate simulated biodistribution data that was then used for radiation dosimetry. These studies emphasized developing a model that described antibody targeting of extravascular or solid tumors. Accordingly, since the models incorporated antibody extravasation into the interstitial space of tissues, relatively complex (3–10 compartments) models have been used. In several cases, due to the negligible effect a low solid tumor burden would be expected to have on gross antibody kinetics, tumors were not specifically incorporated into the models.

By using M195 against acute myelogenous leukemia (AML) as an example, this work focuses on the targeting of hematologically distributed diseases rather than solid tumors. The high and rapidly accessible tumor burden in AML patients requires a model that explicitly incorporates antibody binding to tumor cells. A two-compartment nonlinear model was used to fit the biodistribution data obtained from an administration of trace-labeled antibody. Such an analysis is particularly applicable to disseminated, hematologic diseases rather than solid tumors, since the physiology of antibody targeting is considerably simplified.

METHODS

Patient Biodistribution Data

The characteristics of M195 (anti-CD33) antibody have been previously reported (*7,8*). Details regarding trial design, patient

Received Jun. 10, 1992; revision accepted Oct. 19, 1992.

For correspondence and reprints contact: George Sgouros, PhD, Dept. of Medical Physics, Memorial Sloan-Kettering Cancer Center, 1275 York Ave., New York, NY 10021.

attributes and data collection for the Phase I dose-escalation study of M195 have also been previously reported (*9*). Peripheral leukocyte counts in these patients were suppressed using hydroxyurea. Nonspecific uptake of M195 by the reticuloendothelial system was discounted by comparison with ^{99m}Tc sulfur colloid scans (*9*). The plasma clearance curves obtained in this study were converted from "percent dose per ml plasma" to nanomoles of antibody assuming a distribution volume of antibody, V_d, equal to the plasma volume (3 liters) and to the sum of the liver, spleen and red bone marrow extracellular fluid volumes [0.48, 0.05 and 0.22 liters, respectively (*10*)]. Due to the near absence of a developed capillary basal lamina in the latter three tissues (*3,11,12*), intravenously administered antibody rapidly equilibrates within the extracellular fluid volume of these tissues. The total distribution volume of the antibody will depend upon patient size, the extent to which tumor cells are found in liver, spleen and red marrow and whether splenomegaly or hepatomegaly are evident. A priori corrections to V_d for these variables were not performed; rather, the model fits themselves were relied upon to expose any deficiencies in the starting assumptions. Patient-specific assessments of V_d may be obtained using a trace-labeled irrelevant antibody.

Compartmental Model

The nonlinear, two-compartment model used to fit the biodistribution data is depicted in Figure 1. This model assumes that a given number of antigen sites, Ag_0, are uniformly distributed in a volume, V_d. Antibody is injected into compartment 1 of this model as free antibody, Ab(t). It distributes itself within V_d and binds to available antigen yielding AbAg(t) at a time-dependent rate equal to $k_+/V_d \cdot (Ag_0 - AbAg)$. The differential equations describing these processes are provided in the Appendix (Equations 1 and 2).

Version 30 of the Simulation Analysis and Modeling (SAAM) program developed by Berman et al. (*13*) and supported by the Resource Facility for Kinetic Analysis (University of Washington, Center for Bioengineering, Seattle, WA) operating on a VAX 8810 computer (Digital Equipment Corporation, Maynard, MA) was used to numerically solve and perform parameter fits to these equations.

The total number of antigen sites, Ag_0, was converted to kilograms of tumor burden using 10^4 antigen sites per leukemia blast (*8*) and 10^{12} cells per kilogram (*14*). All antigen-positive cells were assumed to be tumor cells; the known cross-reactivity of M195 with selected other myeloid and monocytic cells (*8*) was ignored. Since each participant of the Phase I study had not previously received mouse antibody, human anti-mouse activity was assumed to be negligible over the duration of data acquisition, and the pharmacokinetic impact of such an immune response to the mouse antibody was not included in this model.

Initial fits to each patient's data were obtained by simulating a single injection of trace-labeled antibody. The parameters obtained for each fit were used as starting values for fitting a compartmental model that also incorporated multiple administrations of unlabeled (cold) antibody at various times following the initial injection of trace-labeled antibody. This was necessary because the patients received such cold antibody while blood samples were still being collected for counting of the initial, trace-labeled administration. The technique used to incorporate cold antibody administrations is depicted by Equations 3 through 5 in the Appendix.

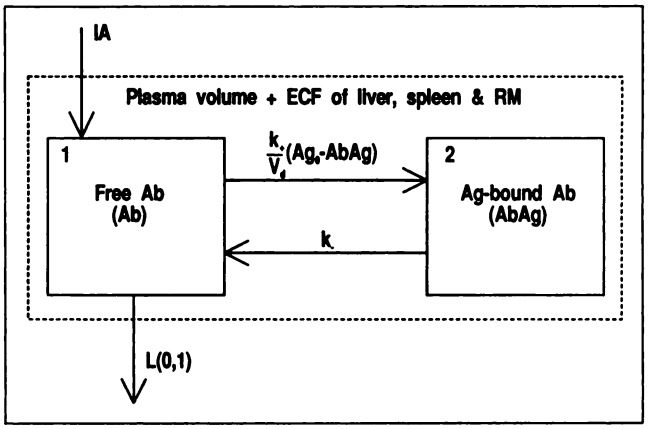

FIGURE 1. The compartmental model used to fit the Phase I biodistribution data. The dotted line represents the 3.8 liter distribution volume of antibody.

Initial Parameter Estimation

Association and dissociation rates (k_+ and k_-, respectively) of typical, high affinity, antibody-antigen interactions have been carefully detailed by Mattes, et al. (*15*). These parameters, performed under physiologic conditions (temperature and pH) for an ovarian carcinoma antigen were used as starting values and adjusted along with the total number of antigen sites (Ag_0) and the total body clearance rate [L(0,1)] to fit the plasma clearance data of Patient 4 (selected because extensive and long-term data were available for this patient). The estimates of k_+ and k_- obtained were 0.5 liter nmole^{-1} h^{-1} and 0.003 h^{-1}, respectively. These values were maintained for all other simulations. Except for Patients 8 and 9, the plasma clearance data for each patient were fit by adjusting Ag_0 and L(0,1). To fit the data from Patients 8 and 9, the antibody distribution volume (V_d) had to be included as an adjustable parameter. The distribution volume for the other patients was fixed at 3.8 liters.

Liver and Spleen Fits

Due to the near absence of a developed capillary basal lamina in the liver and spleen (*11,16,17*), tumor cells within the extracellular space of these tissues were assumed to be directly accessible to intravenously administered antibody (*3*). Correspondingly, a fit to quantitative imaging data for the liver and spleen was obtained by apportioning the antibody in compartments 1 and 2 of the model to each tissue. Since compartment 1 represents free antibody, this distributes within the liver and spleen according to the vascular and extracellular spaces of these tissues. The contents of compartment 2 distributes in an analogous manner according to the distribution of tumor burden. The time-activity curve obtained by quantitative imaging over each organ is, therefore, assumed to consist of two components: the activity due to free antibody in the vascular and extracellular space of each organ, and the activity due to antigen-bound (or tumor-cell associated) antibody. The following equations describe the liver and spleen time-activity curves in terms of model compartments:

$$Q_L(t) = CF \cdot (f_{L1} \cdot Ab(t) + f_{L2} \cdot AbAg(t)) \qquad \text{Eq. 1}$$

$$Q_S(t) = CF \cdot (f_{S1} \cdot Ab(t) + f_{S2} \cdot AbAg(t)) \qquad \text{Eq. 2}$$

where $Q_{L,S}(t)$ is the liver or spleen time-activity curve (cpm), CF is the calibration factor (cpm/nmole), $f_{L1,S1}$ is the fraction of Ab in the vascular and extracellular fluid (ECF) space of either liver or spleen and $f_{L2,S2}$ is the fraction of AbAg in the liver or spleen. As indicated above, the product of f_{L1} or f_{S1} with V_d should yield the vascular and extracellular volume of liver and spleen, respectively. Likewise, multiplying f_{L2} or f_{S2} by the total tumor burden will yield the tumor burden in liver and spleen.

Radionuclide counts for liver and spleen, obtained by whole-body gamma-camera imaging, were divided by the total body counts to yield count ratios. These count ratios were then fit directly to the compartmental model by adjusting the "f" values. This approach eliminated the need to determine the calibration factor. The following equations were used to relate the measured ratio data to the compartmental model:

$$MQ_L(t) = \frac{f_{L1} \cdot Ab(t) + f_{L2} \cdot AbAg(t)}{Ab(t) + AbAg(t)} \quad \text{Eq. 3}$$

$$MQ_S(t) = \frac{f_{S1} \cdot Ab(t) + f_{S2} \cdot AbAg(t)}{Ab(t) + AbAg(t)} \quad \text{Eq. 4}$$

where $MQ_L(t)$ is the measured liver/total body time-activity curve and $MQ_S(t)$ is the measured spleen/total body time-activity curve. It is important to note that by fitting the imaging data for liver and spleen in this manner, the structure of the two-compartment model remains unchanged. All of the parameters defining the compartmental model depicted in Figure 1 and described by Equations 1 through 5 in the Appendix were obtained by fitting the plasma clearance data. These "intrinsic" model parameters were kept fixed while the "f" values were varied to obtain fits to the liver and spleen data.

Although bone marrow biopsy data could be fit to the compartmental model using the approach outlined above for liver and spleen, this was not done for data collected in the Phase I study since only two biopsies were obtained for each patient. By assuming that compartment 1 distributes according to ECF volume and that tumor cells not in the liver or spleen are in the marrow, a biodistribution curve for marrow $[(Q_{RM}(t)]$ may be derived thus:

$$Q_{RM}(t) = \frac{0.22}{3.8} \cdot Ab(t) + (1 - f_{L2} - f_{S2}) \cdot AbAg(t) \quad \text{Eq. 5}$$

As indicated by Equation 5, the antibody in red marrow from compartment 1 was obtained by assuming that the fraction of free antibody in marrow is equal to the red marrow extracellular fluid space [0.22 liter (*10*)] divided by V_d (3.8 liters). The second term in the equation represents antigen-bound antibody. The conservative (i.e., worst-case) assumption is made that, except for tumor cells accounted for by the liver and spleen, all antigen-positive cells are in the red marrow. Equation 5 was used to compare model predictions with the biopsy measurements. The biopsy values reported (*9*) were converted from "ng antibody/gm bone marrow" to "nmole" of antibody by assuming a red marrow weight of 1500 g (*10*) and an antibody molecular weight of 150 kD.

A measure of the uniqueness of each model fit and the resulting parameter estimates were obtained from the SAAM program in the form of standard deviations for the parameter values (*13*). Standard deviation estimates that are large compared to parameter values generally reflect the nonuniqueness of the solution (*13*).

Organ Dosimetry

The mean absorbed dose to the liver, spleen and red marrow was calculated according to the Medical Internal Radiation Dose (MIRD) Committee formalism (*18–20*). The cumulated radioactivity (i.e., total number of radionuclide transformations) for each compartment of the model was obtained by multiplying the contents of each compartment as a function of time by the radiolabeled antibody specific activity and by an exponential decay term corresponding to the decay half-life of ^{131}I. The SAAM UF function was then used to integrate the resulting time-activity curves (*21*). The cumulated activity in each compartment of the model was apportioned to liver, spleen and red marrow in accord with Equations 1, 2 and 5.

Unassigned cumulated activity was assumed to be uniformly distributed throughout the body. Only the self-dose and the total body contributions were included in the absorbed dose calculations for the liver, spleen and red marrow.

Tumor Cell Dosimetry

The cumulated radioactivity in compartment 2 of the model, $\tilde{A}_{II}$, corresponds to the total number of radionuclide transformations that occur while the radiolabeled antibody is bound to a cell-surface, tumor-associated antigen. Dividing $\tilde{A}_{II}$ by the total number of tumor cells yields the cumulated activity ascribed to a single tumor cell. The total number of tumor cells was obtained from the model-derived estimate of Ag_0, using 10^4 antigen sites per cell (*8*).

The absorbed dose at the center of an isolated tumor cell (i.e., one which is not subject to a dose contribution from other cells) was obtained by assuming that the single-cell cumulated activity is uniformly distributed on the cell surface. By modeling the tumor cell as a 5 μm radius sphere (*22*), the cumulated activity "density" on its surface was calculated:

$$D(0) = \sigma \cdot \int_0^{2\pi} \int_0^{\pi} K(R) \cdot R^2 \cdot \sin(\theta) \cdot d\theta \cdot d\varphi \quad \text{Eq. 6}$$

where D(0) is the absorbed dose at the center of the cell (Gy), σ is the cell-surface cumulated activity density (Bq s μm^{-2}), K(r) is the dose point-kernel in water for ^{131}I(Gy Bq^{-1} s^{-1}) and R is the radius of the tumor cell (= 5 μm).

Tabulated values of a published point kernel for ^{131}I (*23*) were obtained from Dr. Douglas Simpkin (*personal communication*). The photon dose contribution to the tumor cell from activity on its surface was assumed negligible relative to the electron dose (*24*). Although in sum, the photon dose from sources other than the target cell could be significant, this is not considered in the tumor cell dose calculation since, for ^{131}I, it represents non-specific irradiation (i.e., does not impact the target to normal tissue absorbed dose ratio).

RESULTS

Fit to Plasma

Compartmental model fits to 9 of the 10 Phase I study plasma clearance curves are depicted in Figures 2a–i. Patient 1 was not fit because only four blood clearance values were collected. Table 1 compares the fitted model

parameters with patient measurements. To fit the data from Patients 8 and 9, the antibody distribution volume had to be included as an adjustable parameter. One possible explanation for this may be the relatively high fraction of estimated total tumor burden found in blood for these two patients [33% and 15%, respectively versus a range of 0.1% to 3% for the remaining patients (*9*)]. Such a high concentration of circulating tumor cells may be expected to internalize a higher fraction of the antibody at an early time, thereby yielding an artificially increased V_d.

The total tumor burden values reported (obtained by measuring the percentage of myeloid leukemia blasts in blood and in bone marrow biopsies) are subject to a considerable sampling error (arising primarily from the bone marrow biopsies) and are likely to be underestimates since spleen, liver and extramedullary involvement were not measured (*9*). By including the extracellular fluid space of the liver, spleen and red marrow, model-derived estimates of the total-body tumor burden may represent a closer approximation to the actual tumor burden. With the exception of Patients 6 and 8, the model-derived clearance rates are in general agreement with the reported values. The discrepancy in Patient 8 may be accounted for by the absence of a sufficient number of longer-term data points (Fig. 2g).

Fit to Liver and Spleen

Figures 3a–g depict model fits to liver and spleen quantitative imaging data. The data for Patient 2 were not fit because the measured plasma curve did not cover the time span over which the imaging data were collected; Patient 10 did not undergo quantitative imaging. To obtain the absolute amount of antibody in each organ, the tissue-to-total body count ratio at each time point was multiplied by the total antibody content of the model (compartments 1 + 2). Table 2 lists the spleen and liver tumor burden and the extracellular fluid and vascular volume estimates obtained from the model. In several cases (primarily for the tumor burden estimates), the standard deviation obtained for the fitted values exceeds the fitted value itself. This is strikingly evident for Patient 8, since only two imaging data points were available for this patient. This example illustrates the built-in assessment of fit quality provided by the model. In general, the large standard deviations reflect an inadequacy in the number of measured data points and the resulting nonuniqueness of the solution. Reference Man values for the sum of the extracellular and the vascular volumes for liver and spleen are 0.68 and 0.23 liters, respectively (*10*). The values reported for Patients 3, 5, 6, 7 and 9 are in reasonable agreement with these figures. By comparing the model-derived estimates of Table 2 to Reference Man values, the following qualitative predictions may be made: Patient 3, normal liver and spleen volumes; Patient 4, significant tumor in both liver and spleen, probable splenomegaly; Patient 5, normal liver and spleen volumes; Patient 6, probable hepatomegaly; Patient 7, normal liver and spleen volumes; Patient 9, normal liver and spleen volumes. All six of these retrospective assessments agreed with blinded, qualitative assessments of liver and spleen size obtained by visual examination of the nuclear medicine images.

Figures 4a and b depict the amount of antibody in the red marrow, obtained by biopsy, compared to the corresponding model-derived estimate. (Patients 1, 2, 8 and 10 are not included because of insufficient data.) Recalling that the bone marrow biopsies are subject to a sampling error that is difficult to evaluate and that the model-derived estimates required assumptions that are not intrinsic to the model (Equation 5), one may observe good

TABLE 1
Model-Derived Parameter Estimates Compared to Measured Values

Patient no.	Tumor burden (kg)		Clearance rate (h^{-1})	
	Measured*	Model-Derived†	Measured	Model-Derived
2	0.1	0.16 ± 0.06	0.007	—‡
3	0.1	0.07 ± 0.05	0.014	0.015 ± 0.008
4	0.9	2.4 ± 0.1	0.020	0.024 ± 0.006
5	0.5	0.64 ± 0.06	0.012	0.015 ± 0.001
6	0.9	1.8 ± 0.06	0.009	0.016 ± 0.002
7	0.6	1.8 ± 0.1	0.013	0.017 ± 0.005
8§	1.5	1.7 ± 0.2	0.011	0.020 ± 0.002
9§	0.4	2.5 ± 0.2	0.019	0.017 ± 0.002
10	1.0	0.93 ± 0.04	0.013	0.018 ± 0.001

*From reference 9.
†Except where noted, $k_+ = 0.5\ nM^{-1}, h^{-1}$, $k_- = 0.003\ h^{-1}$, $V_d = 3.8$ liters.
‡Long-term clearance data were unavailable for this patient.
§V_d was also varied to yield 33 ± 12 and 20 ± 41 for Patients 8 and 9, respectively.

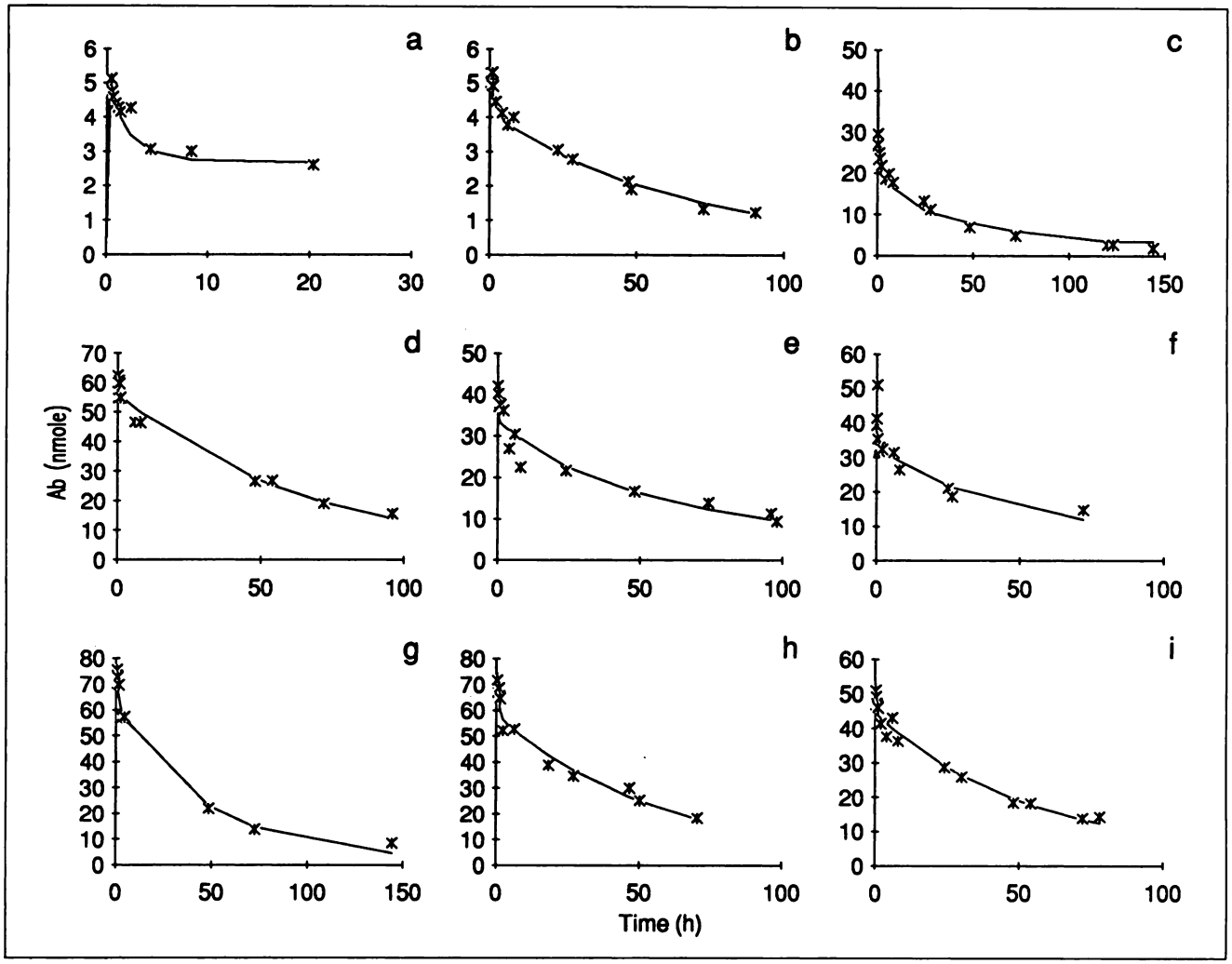

FIGURE 2. The model fits (solid line) to each patients' plasma clearance data (asterisks). Patients 2–10 are depicted consecutively in parts (a) through (i).

agreement between measured and model-derived values for Patients 3, 5 and 7 at the later time point (2–3 days postinjection). At 1 hr, the model-derived estimates for these three patients are approximately two-fold lower than the biopsy data. This systematic difference may reflect an underestimate of the vascular and extracellular fluid volume ascribed to the red marrow. It is noteworthy that of the six patients compared, the three who show good agreement between model-derived versus measured values also exhibit the best plasma clearance fits at early times (data not shown). Although the plasma fit to Patient 9 is also good, it was obtained by including the distribution volume, V_d, as an adjustable parameter.

Organ Dosimetry

Model-derived estimates of the absorbed dose to the liver, spleen and red marrow received by each patient from the ^{131}I tracer study are shown in Table 3. Absorbed dose calculations for Patients 1, 2, 8 and 10 were not performed due to the lack of either sufficient plasma or imaging data. The absorbed dose estimates for the liver and red marrow listed in Table 3 are within the range of the values reported by Scheinberg et al. (*9*). The values reported therein for the liver are 0.8, 0.5, 0.9, 1, 0.8 and 0.5 mGy/MBq for Patients 3, 4, 5, 6, 7 and 9, respectively. The corresponding values for red marrow are 0.7, 1, 5, 7, 3 and 1 mGy/MBq. These values were obtained by directly integrating measured time-activity clearance curves and, in the case of red marrow, by making adjustments for the blood-to-red marrow activity concentration ratio (*9*). The red marrow absorbed dose for Patients 4 and 9 exhibit the largest discrepancy between model-derived and blood pharmacokinetic-based estimates. This is consistent with the discrepancy observed in antibody content between the model estimate and the biopsy measurement (Fig. 4).

Tumor Cell Dosimetry

The absorbed dose to the center of an isolated leukemia blast from Phase I tracer administration of ^{131}I-la-

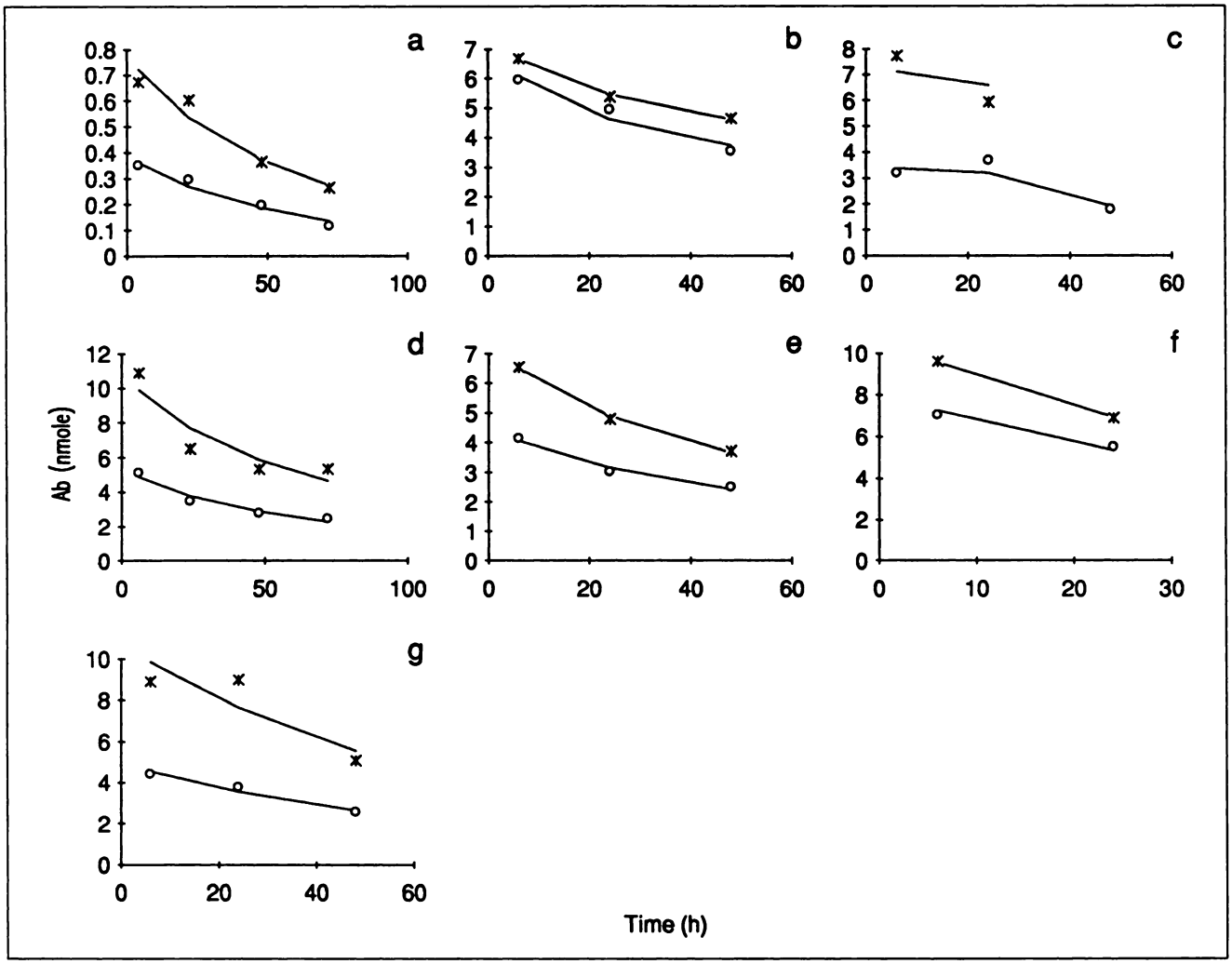

FIGURE 3. Model fits (solid line) to liver (asterisk) and spleen (circle) quantitative imaging data. The fits to Patients 3–9 are depicted consecutively in parts (a) through (g).

beled antibody is 0.02 mGy/MBq for Patients 4, 5, 6, 7 and 9, and 0.07 mGy/MBq for Patient 3. It is important to note that the assumptions used to arrive at these dose estimates represent the worst-case scenario in which the only radiation delivered to the cell is from activity on its surface. Depending upon the tumor cell density, the majority of cells will also receive the average red marrow absorbed dose since they will be subject to a cross-fire component from adjacent cell emissions. The isolated cell dose is important, however, since it reflects the probability of complete tumor-cell eradication (assuming successful targeting of radiolabeled antibody).

TABLE 2
Model-Derived Estimates of Liver and Spleen Characteristics

Patient no.	Tumor burden (kg)		Vascular and ECF volume (liter)	
	Liver	Spleen	Liver	Spleen
3	0.0002 ± 0.002	0	0.68 ± 0.04	0.34 ± 0.03
4	0.19 ± 0.08	0.12 ± 0.08	0.8 ± 0.3	0.95 ± 0.3
5	0	0.01 ± 0.05	0.5 ± 0.3	0.23 ± 0.08
6	0.07 ± 0.07	0.04 ± 0.03	0.76 ± 0.08	0.46 ± 0.08
7	0.02 ± 0.03	0.04 ± 0.03	0.76 ± 0.08	0.46 ± 0.08
8	0.05 ± 2	0.05 ± 2	0.6 ± 3	0.5 ± 3
9	0.1 ± 0.1	0.04 ± 0.02	0.6 ± 0.2	0.28 ± 0.03

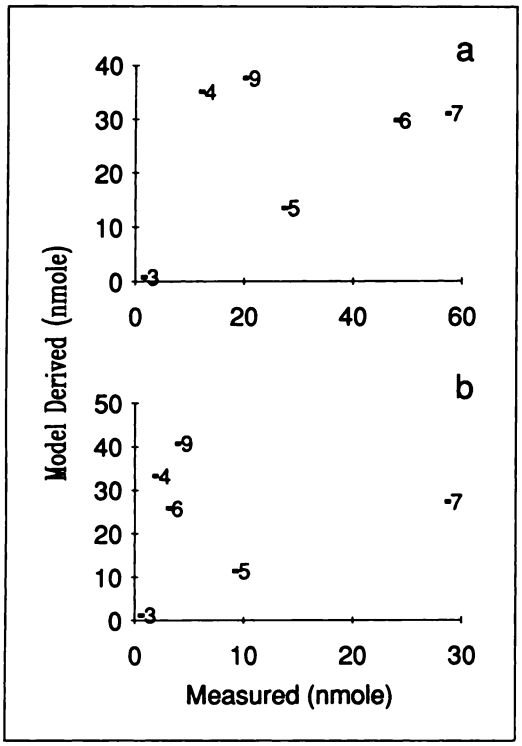

FIGURE 4. Measured (from ref. 9) versus model-derived estimates of antibody in each patient's bone marrow biopsy at 1 hr postinjection (a) and at 3–5 days postinjection (b). Each point is identified by the patient number.

DISCUSSION

Due to the intrinsic radiosensitivity of hematopoietic cancer (*25,26*) and to the rapid access of intravenously administered antibody to tumor-cell associated antigen (*9,27*), radioimmunotherapy of lymphoma and leukemia has yielded significant and reproducible treatment responses (*28–32*). In the treatment of AML, a pilot study of ^{131}I-labeled monoclonal antibody, M195 (*7,8,33,34*), has yielded significant cytoreduction, resulting in up to 99+% decrease in the number of blasts per mm^3 obtained from core biopsies of the bone marrow (*35,36*).

Recalling that the isolated cell absorbed dose estimates represent the worst-case situation in which a circulating tumor cell is irradiated only from beta emissions on its surface, the cytoreduction that has been observed in therapeutic trials may be accounted for by the cross-fire absorbed dose that will yield an additional 0.9–7 mGy/MBq (i.e., the red marrow absorbed dose) for tumor cells in the marrow. It is important to note that the red marrow dose was obtained by assuming that all of the tumor cells not accounted for by the liver and spleen are in the red marrow. In the absence of red marrow biodistribution data, such an estimate places an upper limit on the red marrow dose. The maximum isolated tumor-cell-to-marrow dose ratio was achieved in the patient with the lowest tumor burden. The ratio of red marrow dose-to-tumor cell dose in Patient 3 is approximately 5-fold greater than that in any of the other patients. This result is consistent with the lymphoma and leukemia trials (*28–30,32,35*). In general, treatment efficacy in these trials was improved in patients with a low tumor burden.

TABLE 3
Model-Derived Radiation Absorbed Dose to Liver, Spleen and Red Marrow

Patient no.	Absorbed dose (mGy MBq^{-1})		
	Liver	Spleen	Red marrow
3	0.3	1	0.9
4	1	8	7
5	0.6	2	2
6	1	5	6
7	0.6	4	7
9	0.7	3	7

It is important to note that the proposed model is useful in guiding and providing a quantitative framework for understanding experimental trials of radiolabeled antibodies—not in diminishing the importance of such trials in the optimization of radioimmunotherapy. The model's inability to fit two of the patients' data without including the distribution volume as an adjustable parameter and its systematic underestimate of antibody in the red marrow biopsies at early time illustrates this point. The need to include the distribution volume in two of the fits may be symptomatic of the model's omission of antibody internalization and catabolism. Both in vitro and ex vivo work demonstrates that cell-surface antigen-bound M195 is internalized within several hours (*9,8*). Antibody internalization and catabolism, followed by variable reexpression of antigen sites on the cell surface, would lead to an increase in the effective distribution volume of antibody that is not accounted for by the two-compartment model. That this model deficiency should become apparent for only two of the nine patients may be explained by the observation that a significant fraction of the total tumor burden (33% and 15% in Patients 8 and 9, respectively) was found in blood for these two patients. Early access of administered antibody to such a high fraction of the tumor burden may have highlighted the model's omission of internalization. Since the early time points determine the effective distribution volume of antibody, the increased catabolism of antibody may have been reflected by an artificially increased distribution volume. All other patients exhibited a significantly smaller fraction of their tumor burden in the blood (0.1%–3%). Antibody internalization and catabolism at an early time in such a small fraction of the tumor burden may have had an insignificant impact on the early portion of the plasma clearance curves in these patients. Antibody internalization and catabolism at a later time is probably accounted for by the very slow dissociation rate of antigen-bound antibody ($k_- = 0.003\ h^{-1}$). Although, in the absence of supporting

data, this hypothesis is strictly speculative. It is supported by the observation that the model-derived estimates of distribution volume in Patients 8 and 9 increase in the same direction as the estimates of tumor burden fraction in blood (Patient 8: V_d = 33 liters, blood fraction = 33%; Patient 9: V_d = 20 liters, blood fraction = 15%).

The foregoing discussion reveals the second notable deficiency in a compartmental modeling approach to the analysis of radiolabeled antibody biodistribution data. Implicit in the two-compartment model is the assumption that administered antibody rapidly distributes as free antibody throughout the anatomical distribution volume, V_d. By invoking the fraction of tumor in blood in the foregoing discussion, this assumption is implicitly contradicted. If the antibody truly distributes very rapidly throughout V_d, difficulties associated with the omission of antibody internalization and catabolism would have been independent of the anatomical distribution of tumor burden.

The early therapeutic experience with M195 against acute myelogenous leukemia has resulted in significant reductions in the total tumor burden (*35*). Although not applicable to a tracer study, such successful elimination of tumor cells is expected to reveal a third weakness of the model in not accounting for tumor cell antigen loss during therapy. Evidence demonstrating altered biodistribution of ^{131}I antibody in humans following the administration of large amounts of ^{131}I concurs with such a prediction (*37*).

This work demonstrates that using a relatively simple, two-compartment model to fit patient biodistribution data, one may obtain a set of patient-specific parameters that provide information regarding the patient's clinical status (e.g., total and organ tumor burden). The model-derived total tumor-burden estimate, Ag_0, and model-derived estimates of organ vascular and ECF volumes and tumor burden (i.e., the "f" values) for each of the imaged tissues provide a quantitative basis for assessing the impact of patient variability on a particular therapeutic protocol. Providing such information for each participant of a therapeutic trial would provide a quantitative means for determining the degree to which differences in patient population account for the different response rates observed in various therapeutic trials. Such a distinction would be an important step in establishing a quantitative framework for comparing different therapeutic strategies. By providing an estimate of the residence time or cumulated radioactivity when the labeled antibody is bound to the antigen (compartment 2), and coupling this information with standard tumor cell geometry, a standardized approach to tumor dosimetry may be adopted which would allow for model-based predictions of patient response and for a quantitative intercomparison of different therapeutic strategies using the absorbed dose to an isolated tumor cell as the end-point.

ACKNOWLEDGMENTS

The authors thank Dr. Douglas J. Simpkin of the Department of Radiology at St. Luke's Medical Center, Milwaukee, Wisconsin, for providing the electron point kernel for ^{131}I. George Sgouros is the recipient of a Cancer Research Institute/Jesselson Foundation Fellowship; David A. Scheinberg is a Lucille P. Markey Scholar. This work was supported in part by NIH grants R01-CA55439 and P01-CA33049.

APPENDIX

Compartmental model equations:

$$\frac{dAb(t)}{dt} = -\frac{k_+}{V_d}(Ag_0 - AbAg(t))\,Ab(t) + k_-\,AbAg(t) \quad \text{Eq. 1}$$

$$\frac{dAbAg(t)}{dt} = \frac{k_+}{V_d}(Ag_0 - AbAg(t))Ab(t) - k_-\,AbAg(t) \quad \text{Eq. 2}$$

where Ab(t) is free antibody at time t postinjection (nmole), AbAg(t) is the antigen-bound antibody (nmole), Ag_0 is the initial number of available antigen sites (nmole), k_+ is the association rate constant for antibody-antigen binding (l nmole^{-1} h^{-1}), k_- is the antibody-antigen dissociation rate constant (h^{-1}) and V_d is the anatomical distribution volume of free antibody (liter).

Equations describing an injection of labeled antibody followed by multiple injections of unlabeled antibody:

$$\frac{dAb(t)^*}{dt} = -\frac{k_+}{V_d}\{Ag_0 - (AbAg(t)^* + \sum_j AbAg(t)_j)\}Ab(t)^* + k_-\,AbAg(t)^* \quad \text{Eq. 3a}$$

$$\frac{dAb(t)_j}{dt} = -\frac{k_+}{V_d}\{Ag_0 - (AbAg(t)^* + \sum_j AbAg(t)_j)\}Ab(t)_j + k_-\,AbAg(t)_j \quad \text{Eq. 3b}$$

$$\frac{dAbAg(t)^*}{dt} = \frac{k_+}{V_d}\{Ag_0 - (AbAg(t)^* + \sum_j AbAg(t)_j)\}Ab(t)^* - k_-\,AbAg(t)^* \quad \text{Eq. 4a}$$

$$\frac{dAbAg(t)_j}{dt} = \frac{k_+}{V_d}\{Ag_0 - (AbAg(t)^* + \sum_j AbAg(t)_j)\}Ab(t)_j - k_-\,AbAg(t)_j \quad \text{Eq. 4b}$$

$$Ab(t)_j = \begin{cases} 0 & t < t_j \\ IA_j & t = t_j \end{cases} \quad \text{Eq. 5}$$

where Ab(t)* is labeled antibody (nmole), AbAg(t)* is labeled antigen-bound antibody (nmole), $Ab(t)_j$ is unlabeled antibody from cold administration j (nmole), $AbAg(t)_j$ is unlabeled antigen-bound antibody from cold administration j (nmole), t_j is time of cold antibody administration j (h) and IA_j is the amount of cold antibody administered at t_j (nmole).

REFERENCES

1. Koizumi K, DeNardo GL, DeNardo SJ, et al. Multicompartmental analysis of the kinetics of radioiodinated monoclonal antibody in patients with cancer. *J Nucl Med* 1986;27:1243–1254.
2. Rescigno A, Bushe H, Brill AB, Rusckowski M, Griffin TW, Hnatowich DJ. Pharmacokinetic modeling of radiolabeled antibody distribution in man. *Am J Physiol Imaging* 1990;5:141–150.
3. Eger RR, Covell DG, Carrasquillo JA, et al. Kinetic model for the biodistribution of an ^{111}In-labeled monoclonal antibody in humans. *Cancer Res* 1987;47:3328–3336.
4. Covell DG, Barbet J, Holton OD, Black CDV, Parker RJ, Weinstein JN. Pharmacokinetics of monoclonal immunoglobulin G_1, $F(ab')_2$, and Fab' in mice. *Cancer Res* 1986;46:3969–3978.
5. Sung C, Shockley TR, Morrison PF, Dvorak HF, Yarmush ML, Dedrick RL. Predicted and observed effects of antibody affinity and antigen density on monoclonal antibody uptake in solid tumors. *Cancer Res* 1992;52: 377–384.
6. Zanzonico PB, Bigler RE, Primus FJ, et al. A compartmental modeling approach to the radiation dosimetry of radiolabeled antibody. In: Schlafke-Stelson AT, Watson EE, eds. *Proceedings of the Fourth International Dosimetry Symposium*. Oak Ridge, TN: 1985:421–445.
7. Tanimoto M, Scheinberg DA, Cordon-Cardo C, Hule D, Clarkson BD, Old LJ. Restricted expression of an early myeloid and monocytic cell surface antigen defined by monoclonal antibody M195. *Leukemia* 1989;3: 339–348.
8. Scheinberg DA, Tanimoto M, McKenzie S, Strife A, Old LJ, Clarkson BD. Monoclonal antibody M195: a diagnostic marker for acute myelogenous leukemia. *Leukemia* 1989;3:440–445.
9. Scheinberg DA, Lovett D, Divgi CR, et al. A phase I trial of monoclonal antibody M195 in acute myelogenous leukemia: specific bone marrow targeting and internalization of radionuclide. *J Clin Oncol* 1991;9:478–490.
10. International Commission on Radiological Protection. *Report of the task group on reference man*. ICRP Publication 23, New York: Pergamon Press; 1975.
11. Bloom W, Fawcett DW. *A textbook of histology*, 10th edition. Philadelphia: W.B. Saunders Co.; 1975.
12. Tavassoli M, Yoffey YM. *Bone marrow: structure and function*. New York: Alan R. Liss; 1983.
13. Berman M, Weiss MF. *SAAM Manual*. US DHEW Publication No. (NIH) 78-810, Washington, DC, 1978.
14. Hiddemann W, Clarkson BD, Buchner T, Melamed MR, Andreef M. Bone marrow cell count per cubic millimeter bone marrow: a new parameter for quantitating therapy-induced cytoreduction in acute leukemia. *Blood* 1982;59:216–221.
15. Mattes MJ, Lloyd KO, Lewis Jr JL. Binding parameters of monoclonal antibodies reacting with ovarian carcinoma ascites cells. *Cancer Immunol Immunother* 1989;28:199–207.
16. Dewey WC. Vascular-extravascular exchange of ^{131}I plasma proteins in the rat. *Am J Physiol* 1959;197:423–431.
17. O'Conner SW, Bale WF. Accessibility of circulating immunoglobulins G to the extravascular compartment of solid rat tumors. *Cancer Res* 1984; 44:3719–3723.
18. Loevinger R, Berman M. A revised schema for calculating the absorbed dose from biologically distributed radionuclides. *MIRD pamphlet no. 1, revised*. New York: Society of Nuclear Medicine; 1976.
19. Snyder WS, Ford MR, Warner GG. Estimates of specific absorbed fractions for photon sources uniformly distributed in various organs of a heterogeneous phantom. *MIRD pamphlet no. 5, revised*. New York: Society of Nuclear Medicine; 1976.
20. Snyder WS, Ford MR, Warner GG, Watson EB. "S," absorbed dose per unit cumulated activity for selected radionuclides and organs. *MIRD pamphlet no. 11, revised*. New York: Society of Nuclear Medicine; 1975.
21. Foster DM, Boston RC, Jacquez JA, Zech LA. *The SAAM tutorials: an introduction to using conversational SAAM version 30*. Seattle: Resource Facility for Kinetic Analysis; 1989.
22. Israels MCG. *An atlas of bone-marrow pathology*, 4th edition. New York: Grune and Stratton, Inc.; 1971.
23. Simpkin DJ, Mackie TR. EGS4 monte carlo determination of the beta dose kernel in water. *Med Phys* 1990;17:179–186.
24. Ellett WH, Humes RM. Absorbed fractions for small volumes containing photon-emitting radioactivity. *MIRD pamphlet no. 8*, New York: Society of Nuclear Medicine; 1971.
25. Imai Y, Nakao I. In vivo radiosensitivity and recovery pattern of the hematopoietic precursor cells and stem cells in mouse bone marrow. *Exp Hematol* 1987;15:890–895.
26. Meijne EI, vad der Winden-van Groenewegen RJ, Ploemacher RE, Vos O, David JA, Huiskamp R. The effects of x-irradiation on hematopoietic stem cell compartments in the mouse. *Exp Hematol* 1991;19:617–623.
27. Scheinberg DA, Strand M. Kinetic and catabolic considerations of monoclonal antibody targeting in erythroleukemic mice. *Cancer Res* 1983;43: 265–272.
28. DeNardo SJ, DeNardo GL, O'Grady LF, et al. Pilot studies of radioimmunotherapy of B cell lymphoma and leukemia using I-131 Lym-1 monoclonal antibody. *Antibody Immunoconj Radiopharm* 1988;1:17–34.
29. Press OW, Eary JF, Badger CC, et al. Treatment of refractory non-Hodgkin's lymphoma with radiolabeled MB-1 (Anti-CD37) antibody. *J Clin Oncol* 1989;7:1027–1038.
30. Scheinberg DA, Straus DJ, Yeh SD, et al. A phase I toxicity, pharmacology, and dosimetry trial of monoclonal antibody OKB7 in patients with non-Hodgkin's lymphoma: effects of tumor burden and antigen expression. *J Clin Oncol* 1990;8:792–803.
31. Czuczman MS, Straus DJ, Divgi CR, et al. A phase I dose escalation trial of I-131-labeled monoclonal antibody OKB7 in patients with non-Hodgkin's lymphoma[Abstract]. *Blood* 1990;76(Suppl.1):345.
32. Goldenberg DM, Horowitz JA, Sharkey RM, et al. Targeting, dosimetry and radioimmunotherapy of B-cell lymphomas with iodine-131-labeled LL2 monoclonal antibody. *J Clin Oncol* 1991;9:548–564.
33. Griffin JD, Linch D, Sabbath K, Larcom P, Schlossman SF. A monoclonal antibody reactive with normal and leukemic human myeloid progenitor cells. *Leuk Res* 1984;8:521–534.
34. Peiper SC, LeBoeuf RD, Hughes CB, et al. Report on the CD33 cluster workshop: Biochemical and genetic characterization of gp67. In: Knapp W, Dorken B, Gilkes WR, et al. eds., *Leukocyte Typing IV White Cell Differentiation Antigens*. Oxford: Oxford University Press; 1989:814–818.
35. Schwartz MA, Lovett DR, Redner A, et al. Leukemia cytoreduction and marrow ablation after therapy with I-131-labeled monoclonal antibody M195 for acute myelogenous leukemia (AML) [Abstract]. *Proc ASCO* 1991;10:230.
36. Scheinberg DA, Graham MC, Divgi CR, et al. Myelogenous leukemia and bone marrow ablation with antibody-targeted iodine-131: dosimetry and pharmacology [Abstract]. *Proc ASCO* 1991;10:259.
37. Badger CC, Davis J, Nourigat C, et al. Biodistribution and dosimetry following infusion of antibodies labeled with large amounts of ^{131}I. *Cancer Res* 1991;51:5921–5928.